Nonlinear optics at low powers: Alternative mechanism of on-chip optical frequency comb generation

Andrei S. Rogov* and Evgenii E. Narimanov
Birck Nanotechnology Center, School of Electrical and Computer Engineering, Purdue University, West Lafayette, Indiana 47907, USA
(Received 23 June 2016; published 15 December 2016)

Nonlinear optical effects provide a natural way of light manipulation and interaction and form the foundation of applied photonics, from high-speed signal processing and telecommunication to ultrahigh-bandwidth interconnects and information processing. However, relatively weak nonlinear response at optical frequencies calls for operation at high optical powers or boosting efficiency of nonlinear parametric processes by enhancing local-field intensity with high-quality-factor resonators near cavity resonance, resulting in reduced operational bandwidth and increased loss due to multiphoton absorption. We present an alternative to this conventional approach, with strong nonlinear optical effects at low local intensities, based on period-doubling bifurcations near nonlinear cavity antiresonance and apply it to low-power optical frequency comb generation in a silicon chip.

DOI: 10.1103/PhysRevA.94.063832

I. INTRODUCTION

In the never-ending quest for higher signal processing speeds, optics-based systems represent an attractive research direction since, in contrast to the well-studied area of electronics, the optical domain is perfectly suitable for operation at high frequencies. The basis for any signal processing is manipulation of signals, or light waves, as in the case of optics. Medium nonlinearity provides a means of interaction of different propagating waves with each other and the medium itself.

Two strategies have been traditionally used to enhance nonlinear optical effects: (1) targeting materials with high optical nonlinearities, such as chalcogenide glasses [1,2], silicon [3,4], and AlGaAs [5,6], and (2) employing resonant structures to increase local-field intensity. The choice of material is oftentimes dictated by fabrication limitations and the overall design compatibility requirements. For example, due to its lower cost and direct compatibility with the well-developed complementary metal-oxide semiconductor industry, silicon-based nonlinear photonics has gained a lot of interest in the last decade [4]. On the other hand, resonators offer significant enhancement of local-field intensity at the resonance regime, which allowed for experimental observation of nonlinear optical effects in mode-locked lasers [7,8] and fiber-ring resonators at first [9–11] and then, with the development of microfabrication, in high-quality-factor (Q) microresonators [12–28]. However, boosting local-field intensities with high-Q resonators for enhancing nonlinearity has its disadvantages. First, high intracavity intensities lead to significant multiphoton absorption losses, which makes this resonant approach inapplicable to materials with substantial nonlinear losses, such as silicon at the telecom wavelength of 1550 nm [29]. Second, ultrahigh-Q microresonators, which allow for observation of nonlinear effects at the lowest power, are extremely sensitive to fabrication nonidealities and suffer from poor scalability and on-chip integrability. Finally, high-Q microresonators at the resonance are highly susceptible to external perturbations, up to individual molecules, which is advantageous for nanoparticle detection systems [30–32] but detrimental to many other applications. As we show in this work, nonlinear effects in microresonators can also be observed in the near-antiresonance regime, which, in contrast to the standard resonant approach, naturally implies low intracavity intensity operation and as such could be less prone to the aforementioned disadvantages. Here, the antiresonant operation of a nonlinear cavity excited by continuous-wave (cw) pumping is defined as the case when the total phase detuning of the pump frequency from the closest resonant mode of the cavity is equal to π: $|\phi + \phi_{NL}| = \pi$, where ϕ is the linear contribution and ϕ_{NL} is the nonlinear contribution (intensity dependent). The linear detuning ϕ is calculated in the conditions of low intensity, such that nonlinear effects are negligible and the cavity is considered "cold". The nonlinear contribution ϕ_{NL} is the extra phase accumulated by the intracavity field over one round-trip in the cavity due to the optical Kerr effect.

Effects of nonlinearity on a system dynamics can often be understood by introducing the concept of modulational instability (MI). MI caused by the interplay between nonlinear and dispersive effects has been observed in many areas of physics [33], including nonlinear optics, where it manifests itself as the breakup of cw radiation into a train of ultrashort pulses [34]. When a cw beam propagates through a homogeneous nonlinear dispersive optical medium, anomalous dispersion is required for the modulational instability to occur. However, in the presence of a feedback, as in the case of a resonator system, modulational instability can arise even at normal dispersion [35] and occurs either close to the cavity resonance or close to the cavity antiresonance [36]. Thus, nonlinear effects in resonators should be expected in both the resonance and antiresonance regimes. Motivated by the advantages of low intracavity intensity operation, we study the effects of nonlinearity in a resonator system in the vicinity of the cavity antiresonance and apply this approach to low-power optical frequency comb generation [37,38] in a silicon chip at the telecom wavelength.

Previous work on frequency comb generation has primarily focused on the resonant regime of a high-Q nonlinear cavity [37,38]. In this case the mean-field approximation is valid, and the dynamics can be modeled accurately using either the

*arogov@purdue.edu

modal expansion theory [39] or the Lugiato-Lefever equation (LLE) [35,40–42]. In the present work we are interested in the antiresonant regime of a cavity in which the system exhibits period-doubling behavior, which has been observed to occur in fiber-ring resonators [43–46]. The mean-field models cannot be applied to the kind of period-doubling instabilities whose origin lies in the inhomogeneity of the pump field and which cause significant changes in the intracavity field between consecutive round-trips. For that reason, we resort to using the Ikeda map [47,48] and solving numerically the nonlinear Schrödinger (NLS) equation [34,49,50].

II. RESULTS

A. Alternative mechanism (single-resonator system)

In the antiresonant regime, the nonlinear dynamics of the single-resonator system is affected by period-doubling instabilities [36]: an increased effective nonlinearity in the resonator brakes the system integrability, which results in period-doubling transition to chaos [47,48]. If cw states are considered stable period-1 states, period-doubling bifurcations lead to the formation of regions in the system parameter space with stable states of higher periods, states with multiple wave amplitude values. The existence of higher-period stable states leads to switching in the time domain: the system traverses the set of allowed stable wave amplitude values in sequence switching between them within the system characteristic time period (round-trip time in the resonator). Periodic switching in the time domain translates to the comb spectrum in the frequency domain. Therefore, frequency comb generation can be achieved in the antiresonant regime of the cavity owing to the existence of period-doubling instabilities.

As we pointed out earlier, a cavity is in the antiresonant regime if the overall phase detuning $|\phi + \phi_{NL}|$ of the pump frequency from the cavity nearest resonance mode is equal to π. Therefore, there are two ways to reach the antiresonant regime. In the first approach, the pump is tuned into one of the "cold-cavity" resonances (linear phase detuning $\phi \approx 0$). Then, the nonlinear phase shift ϕ_{NL} caused by the increased intracavity intensity pushes the cavity into antiresonance. This approach requires significant nonlinear phase shift to be accumulated per every round-trip in the cavity, thus leading to high intracavity intensities ($\phi_{NL} \approx \gamma L P \approx \pi$) necessary to reach antiresonance and period-doubling bifurcations [51].

On the other hand, if the pump was initially tuned into one of the cold-cavity antiresonances (linear phase detuning $\phi \approx \pi$), little nonlinear phase shift and low intracavity intensity ($\phi_{NL} \approx \gamma L P \ll \pi$) are required for the system to reach the antiresonant regime. As a result, period-doubling bifurcations and frequency comb generation in particular, in principle, could be achieved at close to zero intracavity intensities. For real applications low intracavity power means low multiphoton absorption losses. This is the key idea behind the mechanism we propose.

In order to illustrate the main features of the suggested mechanism, we first consider a single-resonator system without group-velocity dispersion (GVD), with a microring resonator coupled to the waveguide [Fig. 1(a)] used both to pump the resonator and to direct the output signal. A dispersion-free

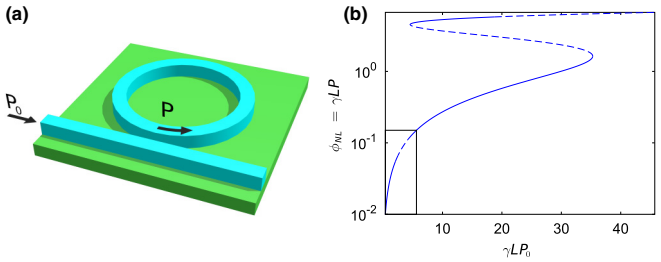

FIG. 1. (a) Schematics of the microring resonator system. (b) Period-1 stable (solid line) and unstable (dashed line) states of the intracavity power P at different values of the input power P_0 with the highlighted first instability region (black rectangle contour). The simulation data were obtained for a resonator with ring radius $R = 10\ \mu$m, $\kappa^2 = 0.1$, $\phi = \pi - 0.14$, $\alpha = 0.7$ dB/cm, and TPA as in silicon near $\lambda = 1550$ nm.

system allows us to apply a simpler, map-based approach for its analysis. Then we perform a full spatiotemporal numerical modeling of the nonlinear dispersive system to study the effects of finite GVD on the proposed mechanism.

Throughout the analysis, we take two-photon absorption (TPA) into consideration. However, it is neither essential nor beneficial for our approach to apply. The motivation behind including TPA in the model is to provide a quantitative connection to the experiments with materials where TPA is present or cannot be neglected, such as silicon at 1550 nm.

The wave propagation over one round-trip of the resonator, assuming a single spatial mode, is governed by the well-known NLS equation [34,49,50]

$$\frac{\partial A}{\partial z} = i\gamma(1+ir)|A|^2 A - \frac{i\beta_2}{2}\frac{\partial^2 A}{\partial T^2} - \frac{\alpha}{2}A, \tag{1}$$

where $A = A(z,T)$ is the normalized wave-packet amplitude ($|A|^2$ has units of power), γ is the nonlinearity coefficient, r is the TPA coefficient ($r \approx 0.1$ for silicon at 1550 nm), β_2 is the group-velocity-dispersion coefficient, α is the power attenuation constant, and $T \equiv t - z/v_g$ is time in the frame of reference moving with the wave packet along the circumference of the ring at the group velocity v_g. Without GVD, Eq. (1) is reduced to

$$\frac{\partial A}{\partial z} = i\gamma(1+ir)|A|^2 A - \frac{\alpha}{2}A \tag{2}$$

and has an analytic solution [49]

$$A(L,T) = A(0,T)\frac{\exp\left(-\frac{\alpha}{2}L\right)}{\sqrt{1+2r\gamma\tilde{L}|A(0,T)|^2}} \times \exp\{i\ln[1+2r\gamma\tilde{L}|A(0,T)|^2]/(2r)\}, \tag{3}$$

where

$$\tilde{L} = \frac{1-\exp(-\alpha L)}{\alpha}. \tag{4}$$

The coupling of the resonator to the waveguide can be modeled by the matrix equation [52]

$$\begin{bmatrix} b(t) \\ d(t) \end{bmatrix} = \begin{bmatrix} \tau & \kappa \\ -\kappa^* & \tau^* \end{bmatrix} \begin{bmatrix} a(t) \\ c(t) \end{bmatrix}, \tag{5}$$

where τ and κ are, respectively, the amplitude transmission and coupling coefficients for the coupler between the microring and the waveguide, $a \equiv A(z = L)$ (L is the circumference of the resonator) and $b \equiv A(z = 0)$, while the amplitudes c and d correspond to the field amplitudes at the "input" and "through" ports of the waveguide. The coupling matrix is unitary, so that $|\tau|^2 + |\kappa|^2 = 1$. For the single-resonator system [Fig. 1(a)], the cw driving field $c(t) \equiv c = \text{const}$ from the pump is coherently added through the coupler every round-trip to the wave circulating in the ring. From Eq. (5) we find that the intracavity field $b^{(n+1)}(t)$ at the beginning of $(n + 1)$th round-trip can be related to the field $a^{(n)}(t)$ at the end of the nth round-trip as

$$b^{(n+1)} = \tau a^{(n)} \exp(i\phi) + \kappa c, \tag{6}$$

where ϕ is the linear phase detuning of the pump frequency from the cavity nearest resonant mode.

The evolution of the intracavity field through one round-trip in the resonator is described by Eq. (3) and in terms of round-trip variables takes the form

$$a^{(n)} = b^{(n)} \frac{\exp\left(-\frac{\alpha}{2}L\right)}{\sqrt{1 + 2r\gamma\tilde{L}|b^{(n)}|^2}} \times \exp[i \ln(1 + 2r\gamma\tilde{L}|b^{(n)}|^2)/(2r)]. \tag{7}$$

The initial condition (6) together with the intracavity evolution equation (7) constitutes a finite-dimensional Ikeda map [47,48], which describes the dynamics of a ring resonator at zero GVD. Stability analysis of the map reveals that the system has multiple regions of period-1 stable and unstable states [Fig. 1(b)]. However, it is the very first instability region that allows for period-1 unstable states to exist at both the lowest intracavity power P and the lowest input power P_0, which is achieved when the resonator is tuned into the vicinity of antiresonance. At the point where the period-1 state loses stability, the system undergoes a period-doubling bifurcation which leads to the formation of period-2 stable state. This dynamics is illustrated in Fig. 2(a), which depicts the lowest-power period-2 bubble. The originally stable period-1 mode corresponding to the time-independent power inside the ring [solid blue line in Fig. 2(a)] eventually loses stability with increasing power, and the system switches to a new period-2 stable mode, a state with the period $2T_c$ ($T_c = L/v_g$ is the round-trip time) corresponding to two ring round-trips [closed red loop with circles in Fig. 2(a)]. At this point, the steady-state power in the microring is no longer time independent, and the switching between the two power levels occurs [Fig. 2(b)], leading to multiple subbands in the power spectrum and frequency comb generation [Fig. 2(c)].

However, with a finite GVD present in the system, the dynamics of the ring resonator cannot be described by a finite-dimensional map, and the evolution of the intracavity field must be found by integrating the NLS equation (1). We solve numerically the NLS equation with the initial condition (6) with the finite-difference time-domain (FDTD) Hopscotch method [53]. We seek a numerical solution for $A(z,t)$ at a set of points z_m, t_k on a rectangular grid in the z,t plane, where $z_m = m\Delta z, t_k = k\Delta t$, Δz is the increment in z, and Δt is the increment in t. The time step Δt is chosen to be

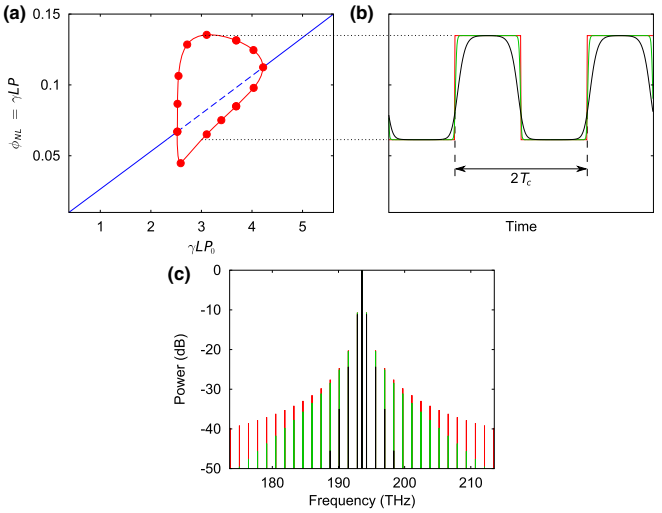

FIG. 2. (a) Bifurcation diagram of the first period-1 instability region [black rectangle contour in Fig. 1(b)] for the states of the intracavity power P at different values of the input power P_0. Fixed points of period 1 and period 2 form the blue line and the red closed loop with circles, respectively. Solid lines represent stable fixed points; dashed lines represent unstable fixed points. (b) Corresponding wave forms and (c) power spectra inside the microring resonator. The red (dark gray) curve in (b) and (c) represents the case of zero GVD; green (light gray) and black curves correspond to the weak ($\beta_2 L/T_c^2 = 1 \times 10^{-5}$) and strong ($\beta_2 L/T_c^2 = 3 \times 10^{-4}$) normal GVD, respectively. The simulation data were obtained for a resonator excited at $\lambda = 1550$ nm ($f \approx 194$ THz) with the scaled input power $\gamma L P_0 = 3$, $\kappa^2 = 0.1$, $\phi = \pi - 0.14$, linear losses $\alpha = 0.7$ dB/cm, TPA as in silicon near $\lambda = 1550$ nm, and ring radius $R = 10\,\mu$m.

large enough to provide a sufficient frequency window for the generated comb spectrum. Step Δz is adjusted to provide the required accuracy. The initial condition has a feedback with the time delay equal to the round-trip time in the resonator. For that reason the numerical integration is performed iteratively, covering $(K - M)$ points in time per pass, where K and M are the number of steps per one round-trip in t space and z space, respectively.

Note that the numerical approach of solving the NLS equation we apply in this work is substantially different from the common one (see, e.g., [14]), which is based on iterations with the split-step Fourier method. The reason for this is that the discrete Fourier transform with the temporal window span of the single round-trip time T_c cannot be applied here since the minimum period of observed states is $2T_c$. Instead, we use the FDTD method [53] to solve numerically the NLS equation with the initial condition defined by the coupling between the waveguide and the resonator.

As expected, the numerical solution shows that the instantaneous switching demonstrated earlier without GVD is replaced by smooth transitions [Fig. 2(b)] in the case of normal GVD. Dispersion acting together with Kerr nonlinearity effectively limits the frequency comb spectrum: the stronger the GVD is, the less frequency components are visible [Fig. 2(c)].

It should be emphasized that the proposed mechanism of frequency comb formation is qualitatively different from the well-known approach [12,16,24]. According to the standard

picture, all comb sidebands are formed at multiple or single free spectral ranges (FSR) Δf away from the pump [16]. In contrast, in the suggested mechanism, the first harmonic is generated at $f_1 = \frac{\Delta f}{2} = \frac{1}{2T_c}$ away from the pump frequency, although the higher harmonics follow single FSR spacing [Fig. 2(c)].

Note that the bifurcation from the period-1 to the period-2 stable state (threshold point for frequency comb generation) takes place at the nonlinear phase shift per round trip $\phi_{NL}^{Th} \equiv \gamma L P^{Th} \approx 0.06 \ll 1$ [Fig. 2(a)]. Moreover, our analysis shows that the threshold intracavity power can be further decreased: $\phi_{NL}^{Th} \equiv \gamma L P^{Th} \sim \kappa^2$, with the optimally tuned linear phase detuning $\phi \sim \pi - \kappa^2$, and the intracavity linear losses are negligibly small compared to the nonlinear ones (valid approximation for the system with the parameters given in Fig. 2). Since the TPA-related loss is proportional to the intracavity power and other multiphoton absorption processes exhibit even stronger power dependence, nonlinear losses are negligible, and linear losses become the limiting factor for the threshold intracavity power.

However, even though the intracavity power threshold can be low, the input power threshold P_0^{Th} is quite high ($\gamma L P_0^{Th} \approx 2.5$) since the resonator is in the antiresonance regime. Low intracavity power leads to the possibility of using materials with high nonlinear losses, such as silicon at the telecom wavelength, while high input power prohibits the single-resonator design discussed above from the practical implementation on a chip. In the next section we resolve this issue.

B. Double-resonator system: A solution to the high-input-power problem

As pointed out earlier, high threshold input power ($\gamma L P_0^{Th} \approx 2.5$) of the single-resonator system complicates or even prevents a practical implementation of the system. This issue can be resolved by introducing another resonator into the system [resonator R_1 in Fig. 3(a)] operating at or near resonance [23,27] and acting as a "preamplifier" between the input waveguide and the nonlinear resonator R_2. To demonstrate the properties of the double-resonator system, we first consider the extra resonator R_1 to be made of a linear optical material, with the case of both resonators made of the same nonlinear medium described in the following section.

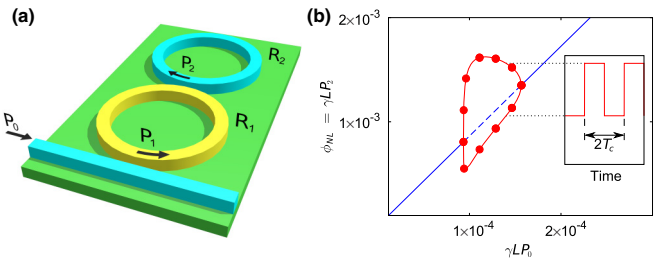

FIG. 3. (a) Schematics of the double-resonator system: R_1 is the linear microring resonator, and R_2 is the nonlinear one. (b) Bifurcation diagram of the first period-1 instability region for the states of the power P_2 inside R_2 at different values of the input power P_0. Fixed points of period 1 and period 2 form the blue line and the red closed loop with circles, respectively. Solid lines represent stable fixed points, and dashed lines represent unstable fixed points. The inset shows wave forms inside R_2 at the scaled input power $\gamma L P_0 = 1.4 \times 10^{-4}$ at zero GVD. The simulation data were obtained for resonators with ring radii $R = 10\ \mu$m, $\kappa_1^2 = 0.01$, $\kappa_2^2 = 0.1$, $\phi_1 = 0$, $\phi_2 = \pi - 1.7 \times 10^{-3}$, $\alpha = 0.7$ dB/cm, and TPA in R_2 as in silicon near $\lambda = 1550$ nm.

Like for the single-resonator system, we obtain the nonlinear map

$$b_2^{(n+1)} = \tau_2 a_2^{(n)} \exp(i\phi_2) + \tau_1 \kappa_2 a_1^{(n)} \exp(i\phi_1) + \kappa_1 \kappa_2 c, \tag{8}$$

$$a_2^{(n)} = b_2^{(n)} \frac{\exp\left(-\frac{\alpha}{2}L\right)}{\sqrt{1 + 2r\gamma\tilde{L}\left|b_2^{(n)}\right|^2}} \times \exp\left[i \ln\left(1 + 2r\gamma\tilde{L}\left|b_2^{(n)}\right|^2\right)/(2r)\right], \tag{9}$$

$$a_1^{(n)} = d_2^{(n)} \exp\left(-\frac{\alpha}{2}L\right), \tag{10}$$

$$d_2^{(n)} = \frac{\tau_2^* b_2^{(n)} - a_2^{(n-1)}}{\kappa_2}, \tag{11}$$

where we assumed the equal round-trip time $T_c = L/v_g$ in both resonators of equal circumference L for simplicity of the analysis, ϕ_1 and ϕ_2 are the linear phase detunings of the pump frequency from the closest resonant modes in the cavities R_1 and R_2, respectively, τ_1 (κ_1) and τ_2 (κ_2) are the amplitude transmission (coupling) coefficients for the coupler between the waveguide and R_1 and between R_1 and R_2, respectively, and γ and r are the nonlinearity and the TPA coefficients, respectively, of the nonlinear resonator R_2.

As before, the stability analysis reveals multiple regions of period-1 stable and unstable states and confirms that the system has a bifurcation from the period-1 to the period-2 stable state when the resonator R_2 is tuned in the vicinity of antiresonance [Fig. 3(b)], as in the case of the single resonator, whereas the resonator R_1 is tuned in the near resonance and provides the required power upconversion between the waveguide and the resonator R_2. More than that, the stability analysis also shows that the double-resonator system is more unstable than the single-resonator system considered earlier, which is beneficial for frequency comb generation. Specifically, adding an extra resonator widens the instability regions and lowers the threshold input power as well as the intracavity powers: $\phi_{NL}^{Th} \equiv \gamma L P_2^{Th} \sim \kappa_1^2 \kappa_2^2$ (against $\phi_{NL}^{Th} \equiv \gamma L P^{Th} \sim \kappa^2$ in the single-resonator system), with the optimally tuned linear phase detuning $\phi_2 \sim \pi - \kappa_1^2 \kappa_2^2$, resonator R_1 in near-resonance regime, and negligible linear loss approximation as before; $\gamma L P_1^{Th} \sim \kappa_2^{-2} \gamma L P_2^{Th} \sim \kappa_1^2$, and $\gamma L P_0^{Th} \sim \kappa_1^2 \gamma L P_1^{Th} \sim \kappa_1^4$ (against $\gamma L P_0^{Th} = \text{const} \approx 2.5$ in the single-resonator system). Therefore, in contrast to the case of the single resonator, the coupling between resonator R_1 and the waveguide in the suggested double-resonator system can be designed so that the threshold input power is orders of magnitude lower [$\gamma L P_0^{Th} \approx 1 \times 10^{-4}$ in Fig. 3(b)], which solves the high-threshold-input-power problem.

However, even though such a double-resonator design could provide frequency comb generation at low input and intracavity powers theoretically, from a practical point of view it would be difficult to fabricate and couple two resonators made from different materials (R_1 is from a highly linear

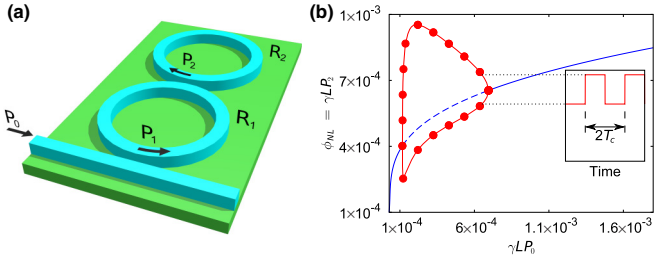

FIG. 4. (a) Schematics of the nonlinear double-resonator system: R_1 and R_2 are nonlinear microring resonators. (b) Bifurcation diagram of the first period-1 instability region for the states of the power P_2 inside R_2 at different values of the scaled input power P_0. Fixed points of period 1 and period 2 form the blue line and the red closed loop with circles, respectively. Solid lines represent stable fixed points, and dashed lines represent unstable fixed points. The inset shows wave forms inside R_2 at the scaled input power $\gamma L P_0 = 6.5 \times 10^{-4}$ at zero GVD. The simulation data were obtained for resonators with ring radii $R = 10$ μm, $\kappa_1^2 = 0.01$, $\kappa_2^2 = 0.1$, $\phi_1 = -1 \times 10^{-2}$, $\phi_2 = \pi - 1.4 \times 10^{-3}$, $\alpha = 0.7$ dB/cm, and TPA as in silicon near $\lambda = 1550$ nm. For the silicon microring waveguide cross-section area of 450 nm × 220 nm, the value of $\gamma L P = 10^{-4}$ corresponds to ≈10 mW of power.

material, such as silica; R_2 is from a nonlinear material, such as silicon) on the same substrate. In the next section we show that the double-resonator system still supports frequency comb generation at low powers even when both resonators are made from the same nonlinear material.

C. Nonlinear double resonator system

Fabricating both resonators from the same nonlinear material would be easier for manufacturing reasons than making them from two different media and, as in the case of silicon, would also be compatible with the standard silicon-based fabrication process. Since the double-resonator system with a linear resonator R_1 is capable of frequency comb generation at low input as well as low intracavity powers, R_1 could be replaced with a nonlinear resonator equivalent to R_2, as shown in Fig. 4(a).

For the nonlinear double-resonator system [Fig. 4(a)] we obtain the nonlinear map

$$b_2^{(n+1)} = \tau_2 a_2^{(n)} \exp(i\phi_2) + \tau_1\kappa_2 a_1^{(n)} \exp(i\phi_1) + \kappa_1\kappa_2 c, \quad (12)$$

$$a_2^{(n)} = b_2^{(n)} \frac{\exp\left(-\frac{\alpha}{2}L\right)}{\sqrt{1 + 2r\gamma\tilde{L}\left|b_2^{(n)}\right|^2}} \times \exp\left[i \ln\left(1 + 2r\gamma\tilde{L}\left|b_2^{(n)}\right|^2\right)/(2r)\right], \quad (13)$$

$$a_1^{(n)} = d_2^{(n)} \frac{\exp\left(-\frac{\alpha}{2}L\right)}{\sqrt{1 + 2r\gamma\tilde{L}\left|d_2^{(n)}\right|^2}} \times \exp\left[i \ln\left(1 + 2r\gamma\tilde{L}\left|d_2^{(n)}\right|^2\right)/(2r)\right], \quad (14)$$

$$d_2^{(n)} = \frac{\tau_2^* b_2^{(n)} - a_2^{(n-1)}}{\kappa_2}, \quad (15)$$

where we assumed the two resonators to be identical, each with the round-trip time $T_c = L/v_g$, circumference L, nonlinearity γ, and TPA r coefficients; $\phi_{1(2)}$, $\tau_{1(2)}$, and $\kappa_{1(2)}$ are defined the same way as before.

As seen from Fig. 4(b), frequency comb generation is possible when the resonator R_2 is tuned in the vicinity of antiresonance and the resonator R_1 is tuned in the near resonance, just as in the previously considered case of the linear preamplifier R_1. The intracavity power in R_1 is sufficiently low ($\gamma L P_1^{Th} \sim 10^{-2}$), so that the multiphoton absorption processes are negligible. Note that the value of the linear phase detuning in R_1 is picked in such a way ($\phi_1 = -1 \times 10^{-2}$) that the resonator operates close to its resonance but does not enter the bistability regime. As could have been expected, with the introduction of nonlinearity in the resonator R_1, the overall system becomes more unstable, which can be observed as broadening of the period-1 instability region, which makes the frequency comb generation regime accessible in a wider range of input powers ($\gamma L P_0 \approx 1 \times 10^{-4}, \ldots, 7 \times 10^{-4}$).

III. DISCUSSION

Now that we have introduced an alternative (antiresonant) mechanism of frequency comb generation, one of the key questions to answer is how it compares with the conventional (resonant) method [12,16,24]. First of all, as was mentioned before, the antiresonant mechanism has a specific spectral signature: the first harmonic is generated at $f_1^{(2)} = \frac{\Delta f}{2} = \frac{1}{2T_c}$ away from the pump frequency for a period-2 state ($f_1^{(n)} = \frac{\Delta f}{n} = \frac{1}{nT_c}$ for a period-n state), while in the resonant approach all harmonics are formed at multiple or single FSR away from the pump. Second, if the comb in the suggested mechanism arises as a consequence of the period-doubling bifurcation, comb generation in the conventional method is connected to the existence of MI gain and cavity solitons. Third, the group-velocity dispersion is the key factor for pattern formation in the resonant approach, while the comb generation with the antiresonant mechanism relies exclusively on the first-order dispersion (group velocity) for pattern formation and nonzero normal GVD only narrows the spectrum.

The existence of a power threshold for parametric oscillation in the resonant regime with anomalous dispersion can be interpreted as a balance between the parametric gain of the NLS equation and the losses in the cavity [12,54]. The threshold power for the antiresonant frequency comb generation is determined by the first period-doubling bifurcation. Figure 5 illustrates the difference in threshold powers for frequency comb generation between the resonant and antiresonant regimes. For the given parameters, the antiresonant method demonstrates the lowest threshold power at low linear losses, while the resonant one demonstrates the lowest threshold power at high losses.

IV. THE ORIGIN OF PERIOD-DOUBLING INSTABILITY

The comb generation in a nonlinear resonator is a special example of pattern formation in nonlinear systems and as such follows the general rules of nonlinear dynamics [55,56]. The onset of the frequency comb formation is related to the loss

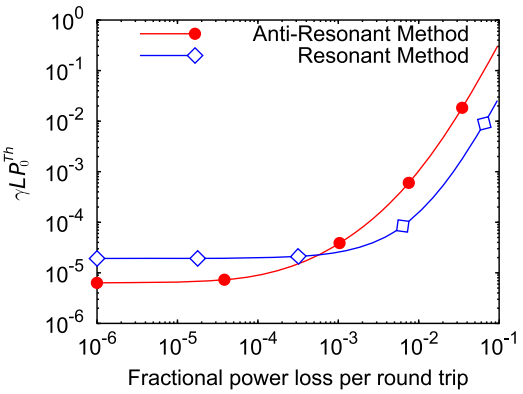

FIG. 5. Input power threshold for frequency comb generation in the resonant (blue curve with open diamonds) and antiresonant (red curve with solid circles) regimes at different levels of linear losses and without nonlinear losses. The simulation data were obtained in the resonant regime for the resonator with $\kappa^2 = 0.01$ and in the antiresonant regime for the nonlinear double-resonator system with $\kappa_1^2 = 0.01$, $\kappa_2^2 = 0.1$. Given the silicon nitride microring waveguide cross-section area of 1.3 μm $\times$ 600 nm and the ring radius of 60 μm [27], the value of $\gamma LP = 10^{-5}$ corresponds to $\approx$20 mW of power.

of stability of the "original" cw state. This loss of stability proceeds via one of the standard bifurcation processes [56], such as the period-doubling bifurcation [55]. To understand the origin of the comb formation in our system, it is therefore necessary to identify the point where nonlinearity will induce this bifurcation.

A cw state of a cavity is stable if perturbations (deviations from the cw amplitude value) diminish with every round-trip in the cavity. If deviations change sign after every round-trip while conserving their amplitude, we observe a possible point of the onset of the period-doubling instability: after the first round-trip intracavity intensity deviates from its cw value, and the next round-trip it returns to its original value. In contrast to the cw mode with a single value of the intracavity intensity, a period-1 state, the new regime has a period of two round-trips with two unique values of the intracavity intensity (period-2 state). Thus, the corresponding coefficient for deviations from the cw state has a special meaning in the stability of the cavity and, when equal to -1 (change of sign without change in deviation intensity), marks the onset of the period-doubling instability. In the literature [56], such an amplification coefficient is known as an eigenvalue of the monodromy matrix for perturbations, and the onset point is known as the period-doubling bifurcation point [55].

In the purely linear and lossless cavity, it is the antiresonance and only the antiresonance point that in the limit of decoupled cavity ($\tau \to 1$) has a real eigenvalue approaching -1. Thus, with finite nonlinearity added to the system, a period-doubling instability region forms in the system phase space around this marginally stable point, and inside of this region frequency comb generation can be observed.

Below, we analytically demonstrate this behavior (eigenvalue $\lambda \to -1$ at antiresonance as $\tau \to 1$). We study the system stability by analyzing the robustness of its cw state to perturbations. Since the physical mechanism behind the onset of period-doubling instability is the same in the single cavity and the double-resonator system, for reasons of clarity we will discuss here the simplest case of a single cavity without losses. The map describing the dynamics of the lossless linear coupled cavity is a special case of the map defined by Eqs. (6) and (7) for $\gamma = 0$ and has a cw solution in the steady state when $b^{(n)} = b = \text{const}$:

$$b = \kappa c + \tau b \exp(i\phi). \tag{16}$$

To check the stability of this cw solution we perturb the steady state slightly such that $b^{(n)} = b + u^{(n)}$. From Eqs. (6) and (7) for $\gamma = 0$ we obtain

$$b + u^{(n+1)} = \kappa c + \tau(b + u^{(n)}) \exp(i\phi). \tag{17}$$

After subtracting Eq. (16) from Eq. (17), we arrive at the linear map for perturbations,

$$u^{(n+1)} = \lambda u^{(n)}, \tag{18}$$

with the eigenvalue

$$\lambda = \tau \exp(i\phi). \tag{19}$$

From Eq. (19) it follows that only at the antiresonance, when $\phi = \pi$, is the eigenvalue real and negative, and in the limit of a decoupled cavity ($\tau \to 1$) it assumes the value of -1. With nonlinearity continuously added to the system, an instability region grows around this point of marginal stability, a region of period-doubling instability, so that period doubling and the related frequency comb generation can be observed at finite coupling, detuning from the cavity antiresonance, and input power.

V. CONCLUSION

In conclusion, we have presented an alternative, antiresonant approach to nonlinear optical processes at low powers and demonstrated its application to low-power optical frequency comb generation in a silicon chip. Theoretical analysis and simulation results showed that the alternative mechanism is capable of operating at low intracavity and input powers and is not suppressed in the presence of two-photon absorption losses in materials such as silicon at the telecom wavelength.

ACKNOWLEDGMENTS

The research was supported by the Air Force Office of Scientific Research (AFOSR) under Grant No. FA9550-12-1-0236 and the Gordon and Betty Moore Foundation. The authors thank Prof. A. M. Weiner for the helpful discussions and comments on the article.

[1] V. Ta'eed, N. J. Baker, L. Fu, K. Finsterbusch, M. R. E. Lamont, D. J. Moss, H. C. Nguyen, B. J. Eggleton, D.-Y. Choi, S. Madden, and B. Luther-Davies, Opt. Express **15**, 9205 (2007).

[2] D.-I. Yeom, E. C. Mägi, M. R. E. Lamont, M. A. F. Roelens, L. Fu, and B. J. Eggleton, Opt. Lett. **33**, 660 (2008).

[3] R. Salem, M. A. Foster, A. C. Turner, D. F. Geraghty, M. Lipson, and A. L. Gaeta, Nat. Photonics **2**, 35 (2008).

[4] J. Leuthold, C. Koos, and W. Freude, Nat. Photonics **4**, 535 (2010).

[5] J. Aitchison, D. Hutchings, J. Kang, G. Stegeman, and A. Villeneuve, IEEE J. Quantum Electron. **33**, 341 (1997).

[6] V. Van, T. Ibrahim, P. Absil, F. Johnson, R. Grover, and P.-T. Ho, IEEE J. Sel. Top. Quantum Electron. **8**, 705 (2002).

[7] D. E. Spence, P. N. Kean, and W. Sibbett, Opt. Lett. **16**, 42 (1991).

[8] T. Brabec, C. Spielmann, P. F. Curley, and F. Krausz, Opt. Lett. **17**, 1292 (1992).

[9] R. M. Shelby, M. D. Levenson, and S. H. Perlmutter, J. Opt. Soc. Am. B **5**, 347 (1988).

[10] M. Nakazawa, K. Suzuki, and H. A. Haus, Phys. Rev. A **38**, 5193 (1988).

[11] S. Coen and M. Haelterman, Opt. Lett. **26**, 39 (2001).

[12] T. J. Kippenberg, S. M. Spillane, and K. J. Vahala, Phys. Rev. Lett. **93**, 083904 (2004).

[13] P. Del'Haye, A. Schliesser, O. Arcizet, T. Wilken, R. Holzwarth, and T. J. Kippenberg, Nature (London) **450**, 1214 (2007).

[14] I. H. Agha, Y. Okawachi, and A. L. Gaeta, Opt. Express **17**, 16209 (2009).

[15] W. Liang, A. A. Savchenkov, A. B. Matsko, V. S. Ilchenko, D. Seidel, and L. Maleki, Opt. Lett. **36**, 2290 (2011).

[16] T. Herr, K. Hartinger, J. Riemensberger, C. Y. Wang, E. Gavartin, R. Holzwarth, M. L. Gorodetsky, and T. J. Kippenberg, Nat. Photonics **6**, 480 (2012).

[17] S. B. Papp and S. A. Diddams, Phys. Rev. A **84**, 053833 (2011).

[18] J. Li, H. Lee, T. Chen, and K. J. Vahala, Phys. Rev. Lett. **109**, 233901 (2012).

[19] L. Razzari, D. Duchesne, M. Ferrera, R. Morandotti, S. Chu, B. E. Little, and D. J. Moss, Nat. Photonics **4**, 41 (2010).

[20] B. J. M. Hausmann, I. Bulu, V. Venkataraman, P. Deotare, and M. Lončar, Nat. Photonics **8**, 369 (2014).

[21] H. Jung, C. Xiong, K. Y. Fong, X. Zhang, and H. X. Tang, Opt. Lett. **38**, 2810 (2013).

[22] J. S. Levy, A. Gondarenko, M. A. Foster, A. C. Turner-Foster, A. L. Gaeta, and M. Lipson, Nat. Photonics **4**, 37 (2010).

[23] S. A. Miller, Y. Okawachi, S. Ramelow, K. Luke, A. Dutt, A. Farsi, A. L. Gaeta, and M. Lipson, Opt. Express **23**, 21527 (2015).

[24] F. Ferdous, H. Miao, D. E. Leaird, K. Srinivasan, J. Wang, L. Chen, L. T. Varghese, and A. M. Weiner, Nat. Photonics **5**, 770 (2011).

[25] Y. Liu, Y. Xuan, X. Xue, P.-H. Wang, S. Chen, A. J. Metcalf, J. Wang, D. E. Leaird, M. Qi, and A. M. Weiner, Optica **1**, 137 (2014).

[26] X. Xue, Y. Xuan, Y. Liu, P.-H. Wang, S. Chen, J. Wang, D. E. Leaird, M. Qi, and A. M. Weiner, Nat. Photonics **9**, 594 (2015).

[27] X. Xue, Y. Xuan, P.-H. Wang, Y. Liu, D. E. Leaird, M. Qi, and A. M. Weiner, Laser Photonics Rev. **9**, L23 (2015).

[28] A. G. Griffith, R. K. W. Lau, J. Cardenas, Y. Okawachi, A. Mohanty, R. Fain, Y. H. D. Lee, M. Yu, C. T. Phare, C. B. Poitras, A. L. Gaeta, and M. Lipson, Nat. Commun. **6**, 6299 (2015).

[29] R. K. W. Lau, M. R. E. Lamont, Y. Okawachi, and A. L. Gaeta, Opt. Lett. **40**, 2778 (2015).

[30] A. M. Armani, R. P. Kulkarni, S. E. Fraser, R. C. Flagan, and K. J. Vahala, Science **317**, 783 (2007).

[31] F. Vollmer and S. Arnold, Nat. Methods **5**, 591 (2008).

[32] J. Zhu, S. K. Ozdemir, Y.-F. Xiao, L. Li, L. He, D.-R. Chen, and L. Yang, Nat. Photonics **4**, 46 (2010).

[33] V. E. Zakharov and L. A. Ostrovsky, Phys. D (Amsterdam, Neth.) **238**, 540 (2009).

[34] G. Agrawal, *Nonlinear Fiber Optics* (Academic Press, USA, 2001).

[35] M. Haelterman, S. Trillo, and S. Wabnitz, Opt. Commun. **91**, 401 (1992).

[36] S. Coen and M. Haelterman, Phys. Rev. Lett. **79**, 4139 (1997).

[37] T. J. Kippenberg, R. Holzwarth, and S. A. Diddams, Science **332**, 555 (2011).

[38] V. Torres-Company and A. M. Weiner, Laser Photonics Rev. **8**, 368 (2014).

[39] Y. K. Chembo and N. Yu, Phys. Rev. A **82**, 033801 (2010).

[40] L. A. Lugiato and R. Lefever, Phys. Rev. Lett. **58**, 2209 (1987).

[41] Y. K. Chembo and C. R. Menyuk, Phys. Rev. A **87**, 053852 (2013).

[42] S. Coen, H. G. Randle, T. Sylvestre, and M. Erkintalo, Opt. Lett. **38**, 37 (2013).

[43] H. Nakatsuka, S. Asaka, H. Itoh, K. Ikeda, and M. Matsuoka, Phys. Rev. Lett. **50**, 109 (1983).

[44] R. Vallée, Opt. Commun. **81**, 419 (1991).

[45] G. Steinmeyer, A. Buchholz, M. Hänsel, M. Heuer, A. Schwache, and F. Mitschke, Phys. Rev. A **52**, 830 (1995).

[46] S. Coen, M. Haelterman, P. Emplit, L. Delage, L. M. Simohamed, and F. Reynaud, J. Opt. Soc. Am. B **15**, 2283 (1998).

[47] K. Ikeda, Opt. Commun. **30**, 257 (1979).

[48] K. Ikeda, H. Daido, and O. Akimoto, Phys. Rev. Lett. **45**, 709 (1980).

[49] L. Yin and G. P. Agrawal, Opt. Lett. **32**, 2031 (2007).

[50] Q. Lin, O. J. Painter, and G. P. Agrawal, Opt. Express **15**, 16604 (2007).

[51] A. S. Rogov and E. E. Narimanov, Opt. Lett. **39**, 4305 (2014).

[52] A. Yariv, Electron. Lett. **36**, 321 (2000).

[53] T. R. Taha and M. I. Ablowitz, J. Comput. Phys. **55**, 203 (1984).

[54] A. B. Matsko, A. A. Savchenkov, D. Strekalov, V. S. Ilchenko, and L. Maleki, Phys. Rev. A **71**, 033804 (2005).

[55] M. J. Feigenbaum, Phys. D (Amsterdam, Neth.) **7**, 16 (1983).

[56] R. L. Devaney, *A First Course in Chaotic Dynamical Systems: Theory and Experiment* (Westview Press, 1992).